The Quantum Magnetism of Individual Manganese-12-Acetate Molecular Magnets Anchored at Surfaces

S. Kahle, Z. Deng, N. Malinowski, C. Tonnoir, A. Forment-Aliaga, N. Thontasen, G. Rinke, S. Rauschenbach, M. Ternes, and K. Kern

At the interface between classical and quantum mechanical description single molecular magnets (SMM) offer novel approaches in information storage, spintronics, and quantum computation. In SMMs spin carrying atoms are arranged within a molecular framework such that their magnetic states can be described as a single giant spin. Mn_{12}, composed of a $Mn_{12}O_{12}$ core surrounded by 16 acetate groups (Fig. 1a), represents a prototypical molecular magnet with a total spin $S = 10$ that, resulting from its large magnetic anisotropy D, has a magnetization reversal barrier height of $-DS^2 = 6$ meV in bulk, enough to produce very long spin relaxation times at low temperatures [1]. Throughout many studies, immobilization of Mn_{12} molecules at surfaces has been found to be difficult, as its fragile structure changes easily upon deposition, thus altering its magnetic properties [2]. In particular the controlled in-vacuo deposition of Mn_{12} is hindered by its thermal instability.

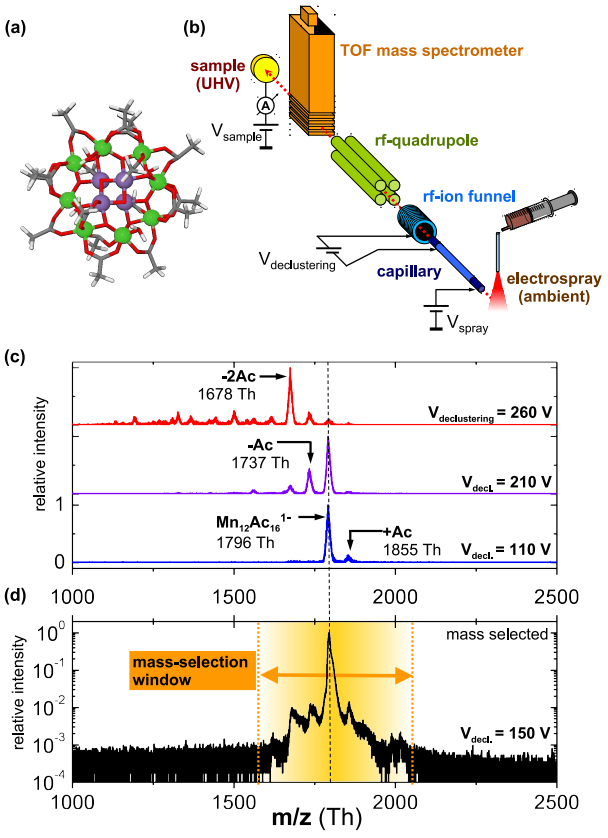

Figure 1: **a**, Structure of the studied molecule $Mn_{12}O_{12}(CH_3COO)_{16}$ (Mn_{12}). Balls represent manganese atoms of two different charge and spin state: Green: Mn^{3+} ($S = 2$), violet: Mn^{4+} ($S = 3/2$). Red (grey, white) sticks represent bonds to oxygen (carbon, hydrogen). All Mn atoms of the same spin state are coupled ferromagnetically while Mn atoms of different spin are coupled antiferromagnetically resulting in a ground state of $S = 10$. **b**, Simplified schematic of the ES-IBD. A solution of Mn_{12} molecules is electrosprayed at ambient conditions and mass selectively deposited onto the sample in ultra high vacuum (UHV) (10^{-10} mbar). **c**, Mass spectra show the intact molecule (1796 Th) and fragments due to acetate loss (1737 Th, 1678 Th) for different declustering potentials. **d**, Mass spectrum of a mass selected beam at $V_{\mathrm{decl.}} = 150$ V for deposition (log scale). The total contamination by fragmented molecules is suppressed to $< 5\%$ intensity.

We have use electrospray ion beam deposition (ES-IBD) as gentle deposition method to bring Mn_{12} molecules on atomically well defined metal and ultra-thin insulating surfaces and study their structure and magnetic properties by scanning tunneling microscopy (STM) and spectroscopy (STS). Fig. 1b illustrates the schematic setup of the ES-IBD system. Time-of-flight (TOF) mass spectra for different declustering potentials ($V_{\mathrm{decl.}}$), a parameter which adjusts the collision energy between the ion beam and the background gas are shown in Fig. 1c. While at low $V_{\mathrm{decl.}}$ a peak corresponding to $Mn_{12}Ac_{17}^{1-}$ is found besides the intact Mn_{12} molecule, at high $V_{\mathrm{decl.}}$ the loss of acetate groups is the main source of defected molecules. To further decrease contamination the Mn_{12} ion-beams were mass selected before deposition using a quadrupole ion guide (Fig. 1d).

After room temperature deposition of Mn_{12} on Cu(001), Au(111), and a mono-layer of BN on Rh(111) we measure STM topographies. On Cu(001) we observe randomly distributed molecules (Fig. 2a) meaning that Mn_{12} is immobile at room temperature. In contrast, on Au(111) the molecules are mobile and can be imaged stably only after cooling down to 40 K. At low coverage they preferably occupy the fcc part of the Au(111) surface reconstruction starting at elbow sites (Fig. 2b). Only after those have been filled the molecules occupy the hcp part of the surface. In contrast to bare metal surfaces, the BN monolayer on Rh(111) is chemically very

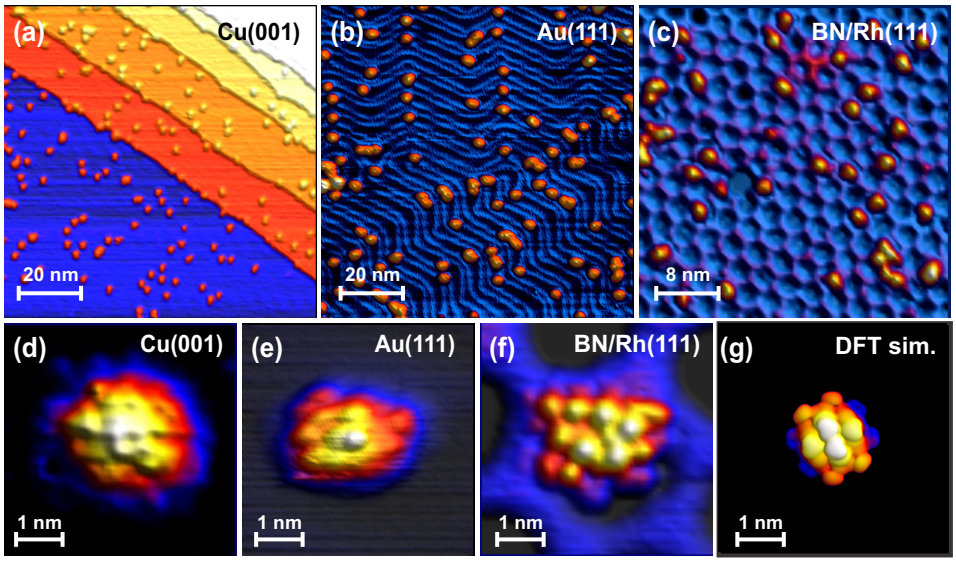

Figure 2: STM topographic images of Mn_{12} molecules deposited on different surfaces. **a**, On Cu(001) immobile molecules are randomly distributed over the surface. **b**, On Au(111) molecules are found preferably at the elbow sites of the herringbone reconstruction. **c**, On the BN/Rh(111) surface molecules adsorb in the depressions of the BN corrugation ($T = 1.5$ K). **d-f**, images of individual molecules reveal an intramolecular structure identified as the acetate groups. Different adsorption geometries can be observed. **g**, comparison with the DFT calculation of the free molecule. Tunneling parameters: **a**: $V = +2$ V, $I = 100$ pA, **b**: +2 V, 80 pA, **c**: +0.9 V, 100 pA, **d**: +2.5 V, 120 pA, **e**: +2 V, 80 pA, **f**: -1 V, 45 pA.

inert and has shown to be an excellent electronic decoupling layer [3]. The deposition of Mn_{12} on the BN surface results in a random distribution of individual molecules in the depressions of the BN corrugation (Fig. 2c).

On all surfaces we identify individual molecules from their size of $(2.3 \pm 0.4) \times (1.9 \pm 0.4)$ nm^2 and a voltage dependent apparent height between 0.25 nm and 0.7 nm. Detailed imaging of the molecules (Fig. 2d–f) shows good agreement to an intact molecule, simulated by density functional theory (DFT) calculation (Fig. 2g). The characteristic sub-molecular structure with lobes of approximately 0.5 nm size corresponds to the acetate groups of the SMM as seen in DFT.

To address the question of whether these SMMs still exhibit their striking magnetic properties, we have applied inelastic spin-flip spectroscopy at low temperature $T = 1.5$ K (fig. 3). We measure the differential conductance $\mathrm{d}I/\mathrm{d}V$ on top of the Mn_{12} molecules and observe symmetric features around the Fermi energy only when the molecule is adsorbed on the thin BN insulator. Spectra in zero and at applied magnetic field perpendicular to the surface show a step-like structure in $\mathrm{d}I/\mathrm{d}V$ which corresponds to peaks in the numerically derivated $\mathrm{d}^2I/\mathrm{d}V^2$ as shown in Fig. 3d. The innermost step is usually the most prominent one and can be found at $1-2$ meV, while the outer steps can be observed in a range up to 16 meV. On bare metal surfaces we do not observe such dominant features presumably due to the quenching of the spin.

To interpret these features we omit for the moment the many spin nature of the system by using the giant spin approximation in which $S = 10$ is fixed. The magnetic anisotropy is responsible for the zero-field splitting of the spin eigenstates in the z-projection m and leads to a degenerate ground state for $|S,m\rangle = |10,-10\rangle$ and $|10,10\rangle$ (Fig. 3b). Excitations of the SMM by the tunneling electrons are detected as increasing differential conductance when the energy of the tunneling electrons is large enough to excite this state and the spin-flip selection rules are obeyed (Fig. 3c). The model with fixed S reduces possible magnetic excitations to changes of m, explaining the inner step of the spectra as the excitation from $|S,m\rangle = |10,\pm10\rangle$ to $|10,\pm9\rangle$.

To cover also excitations which change S we go beyond the giant spin picture and calculate possible spin excitations using a Hamiltonian in which the spin of each individual Mn atom inside the Mn_{12}-molecule interacts with its neighbors and the external magnetic field $\vec{B}$. Calculation of the spin-flip excitations which obey the selection rules shows three low-energy features at 0 T (10 T) of 1.2 (1.8), 5.5 (6.2), and 10.9 (11.6) meV as displayed in Fig. 3e. Comparing the theoretical results with the experimental data reveals good agreement with the observation of 3 peaks but differences in the positions especially at the energetically higher peaks, which is not surprising due to the simplifications of the model in which different adsorption geometries are not taken into account.

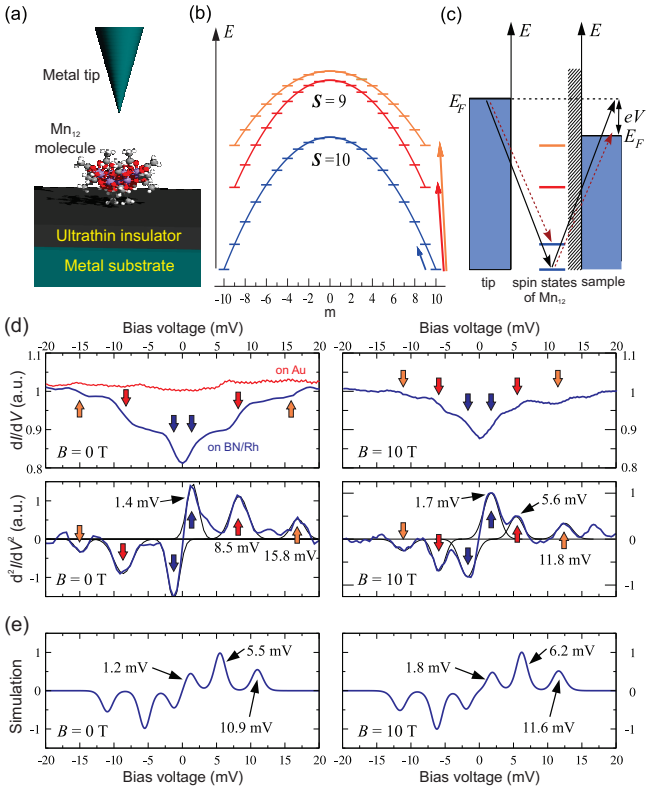

Figure 3: **a**, Schematic of the tunneling geometry. **b**, Schematic energy diagram of a Mn_{12} molecule in the giant spin approximation $H = -DS_z^2$ with $S = 10$ ground state and easy axis anisotropy $D > 0$ without external magnetic fields applied. Arrows indicate possible excitations by interaction with the tunneling electron which obey the spin selection rules $\Delta S = 0, \pm 1$ and $\Delta m = 0, \pm 1$. **c**, Co-tunneling processes between the metal tip and the BN/Rh(111) sample via the Mn_{12} molecule. Full arrows: elastic tunneling; dashed red arrows: inelastic tunneling process which excites the internal spin system of the Mn_{12}. The latter process opens a new conduction channel $\sigma_{\text{inel.}}$ when the bias voltage $e|V|$ exceeds the energy difference between initial and final state and contributes to the total differential conductance $\sigma = \sigma_{\text{el.}} + \sigma_{\text{inel.}}$. **d**, Typical dI/dV and d^2I/dV^2 spectra ($T = 1.5$ K) of a Mn_{12} molecule adsorbed on a BN/Rh(111) surface at $B = 0$ T (left) and $B = 10$ T (right) reveal low energy spin-flip excitations which manifest themselves as steps (peaks) in the dI/dV (d^2I/dV^2) spectrum (blue lines). For comparison Mn_{12} on Au(111) does not show these features (red line in the top left panel). **e**, Simulated d^2I/dV^2 spectra.

In Fig. 3d typical experimental spectra are shown. The lowest excitation can be found in these examples at 1.4 meV (1.7 meV at 10 T) corresponding to a change of the m quantum number by one. The excitations observed at higher energy are due to an additional change of the total spin S of the molecule. For the latter several spin-configurations are possible and are the origin of the two energetically higher excitations observed at $4-9$ meV and $11-16$ meV, respectively. These excitations spread over relatively large range for different molecules presumably due to conformational changes that affect the fragile ligand field of Mn_{12} when adsorbed in different geometries on the surface.

At high tunneling rates, in which the average time between two tunneling events is shorter than the lifetime of the excited state, one expects the pumping into states with higher energy. The lifetime of the excited states can be estimated by the linewidth of the peaks in d^2I/dV^2 to be $2-4$ ps. Thus, spin pumping would require tunneling currents of the order of 100 nA, which is too high for the fragile ligands of the molecule.

In summary, we have demonstrated the controlled deposition of fragile Mn_{12} SMMs on metallic and thin-insulating surfaces and the feasibility of preserving the quantum magnetism of Mn_{12} on thin insulating layers such as BN. ES-IBD and local probe techniques such as STM are ideally suited for the preparation of complex molecular nanostructures and studying their properties. The added value provided by the combination of the two techniques is that the local electronic and magnetic properties derived from STM and STS investigations can be linked directly to a chemical structure, well characterized from the fully controlled, gentle deposition process that can be applied even to fragile molecules such as Mn_{12}. Our work provides access to atomic-scale studies of individual SMMs and their intriguing behavior, opening the pathway to experimentally address characteristics like tunneling of magnetization, lifetime of magnetization, or intermolecular coupling of magnetic moments.

References:

[1] *Sessoli, R., D. Gatteschi, A. Caneschi and M.A. Novak* Nature **141**, 365 (1993)

[2] *Rogez, G., B. Donnio, E. Terazzi, J.L. Gallani, J.P. Kappler, J.P. Bucher and M. Drillon* Adv. Mater. **21**, 4323 (2009)

[3] *Bose, S., A.M. García-García, M.M. Ugeda, J.D. Urbina, C.H. Michaelis, I. Brihuega and K. Kern* Nature Mater. **9**, 550 (2010)

In collaboration with:

D. Le, V. Turkowski, and T. S. Rahman (University of Central Florida, Orlando, United States)